Exp Fluids (2017) 58:134
DOI 10.1007/s00348-017-2412-0

REVIEW ARTICLE

A review of wind turbine-oriented active flow control strategies

Sandrine Aubrun[1,2] · **Annie Leroy**[1] · **Philippe Devinant**[1]

Received: 19 April 2017 / Revised: 21 July 2017 / Accepted: 31 July 2017 / Published online: 5 September 2017

Abstract To reduce the levelized cost of energy, the energy production, robustness and lifespan of horizontal axis wind turbines (HAWTs) have to be improved to ensure optimal energy production and operational availability during periods longer than 15–20 years. HAWTs are subject to unsteady wind loads that generate combinations of unsteady mechanical loads with characteristic time scales from seconds to minutes. This can be reduced by controlling the aerodynamic performance of the wind turbine rotors in real time to compensate the overloads. Mitigating load fluctuations and optimizing the aerodynamic performance at higher time scales need the development of fast-response active flow control (AFC) strategies located as close as possible to the torque generation, i.e., directly on the blades. The most conventional actuators currently used in HAWTs are mechanical flaps/tabs (similar to aeronautical accessories), but some more innovative concepts based on fluidic and plasma actuators are very promising since they are devoid of mechanical parts, have a fast response and can be driven in unsteady modes to influence natural instabilities of the flow. In this context, the present paper aims at giving a state-of-the-art review of current research in wind turbine-oriented flow control strategies applied at the blade scale. It provides an overview of research conducted in the last decade dealing with the actuators and devices devoted to developing AFC on rotor blades, focusing on the flow phenomena that they cause and that can lead to aerodynamic load increase or decrease. After providing some general background on wind turbine blade aerodynamics and on the atmospheric flows in which HAWTs operate, the review focuses on flow separation control and circulation control mainly through experimental investigations. It is followed by a discussion about the overall limitations of current studies in the wind energy context, with a focus on a few studies that attempt to provide a global efficiency assessment and wind energy-oriented energy balance.

List of symbols

a	Axial velocity reduction factor on blade airfoil
a'	Radial velocity increment on blade airfoil
$c(r)$	Local airfoil chord at radial position r (m)
c_μ	Momentum coefficient
$\dot{m}_{\text{inj}}$	Injected mass flow rate (kg/s)
v_{inj}	Injection velocity (m/s)
r	Radial position on the blade (m)
$C_{\text{D}}(r)$	Local airfoil drag coefficient value at radial position r
$C_{\text{L}}(r)$	Local airfoil lift coefficient value at radial position r
$C_{\text{L}\alpha}(r)$	Lift curve slope in the linear region of $C_{\text{L}}(r)$
C_{T}	Thrust coefficient
D	Wind turbine rotor diameter (m)
$L(r)$	Local airfoil lift value at radial position r (N/m)
$R = \frac{D}{2}$	Wind turbine rotor radius (m)
T	Thrust force (N)
U_∞	Upstream time-averaged velocity (m/s)
U_{hub}	Upstream time-averaged velocity at hub height (m/s)
$U_{\text{rel}}(r)$	Relative incoming flow velocity on airfoil at radial position r (m/s)
$\alpha(r)$	Aerodynamic airfoil angle of attack at radial position r (°)

✉ Sandrine Aubrun
sandrine.aubrun@ec-nantes.fr

[1] Univ. Orléans, INSA-CVL, PRISME, EA 4229, 8, RUE Léonard de Vinci, 45072 Orléans cedex 2, France

[2] Present Address: Ecole Centrale de Nantes, LHEEA, 1, rue de la Noe, 44300 Nantes, France

$\alpha_0(r)$	Airfoil zero lift angle of attack at radial position r (°)
$\beta_{\text{twist}}(r)$	Blade twist (°)
β_{pitch}	Collective blade pitch setting (°)
$\lambda = \frac{\Omega R}{U_\infty}$	Wind turbine tip speed ratio
Ω	Wind turbine rotor rotational velocity (rad/s)

1 Introduction

To reduce the levelized cost of energy (LCoE), the energy production, robustness and lifespan of horizontal axis wind turbines (HAWTs) have to be improved to ensure optimal energy production and operational availability during periods longer than 15–20 years. HAWTs operate in a very hostile environment for energy production and durability, since the wind conditions they encounter in the atmospheric boundary layer are strongly inhomogeneous and unsteady.

HAWTs are therefore subject to unsteady wind loads which are responsible for combinations of unsteady mechanical loads with characteristic time scales from seconds to minutes. The wind conditions can become even more hostile when HAWTs are arranged in parks, since the HAWT wakes, which are characterized by a velocity deficit and production of turbulence, can impact other wind turbines. When not properly managed, these working conditions may lead to severe transitional overloads as well as fatigue cracks on the blades after only 5 years of operation. Alleviating the impact of upstream wind fluctuations would lead to more sustainable life conditions for the rotors, enabling design optimization and material savings and inducing improved economics and reduced LCoE. According to the Long-term Research Agenda by the *European Academy of Wind Energy* (van Kuik et al. 2016) and to the Strategic Research and Innovation Agenda by the *European Technology and Innovation Platform on Wind Energy* (ETIP Wind 2016), this can be achieved by controlling the aerodynamic performance of HAWT rotors in real time to compensate the overloads.

Concurrently with load mitigation, it may also be relevant in specific situations, such as during start-up, to improve the instantaneous power performance by locally increasing the aerodynamic performance of blade sections.

Some even consider that actuation on blades could replace pitch control on offshore HAWTs regulated by stall (where the noise impact is not relevant), using the separation location on the suction side as a control parameter of the aerodynamic performance. This could therefore transform a passive control such as stall regulation into an active one. An additional benefit could also be expected on the HAWT start-up velocity, by assisting the start-up process with active flow control (AFC) on blades. These possible applications imply studying AFC efficiency for a wide Reynolds number range (10^5–10^7).

The standard way to improve aerodynamic performance and to reduce load fluctuations on current HAWTs is based on mechanical pitch control, modifying the overall blade pitch, using the instantaneous wind velocity measurement at the hub location or instantaneous electrical power as an input. The implementation of fast response collective, then individual, pitch control systems increases the operating flexibility of the rotor, since it optimizes the pitch angle of the blades at a time scale of 10 s and can mitigate part of the load fluctuations due to wind fluctuations. Mitigating the load fluctuations and optimizing the aerodynamic performance at higher time scales need the development of fast-response AFC strategies located as close as possible to the torque generation, i.e., directly on the blades. As discussed in Barlas and van Kuik (2010), progress in applying rotor control for HAWTs has benefited from many relevant research studies and has achieved results in the aerospace field. Up to now, however, no AFC strategy has been integrated in industrial HAWTs. Only passive control, such as vortex generators located close to the root in low torque production areas of the blades is used. At the prototype stage (Technology Readiness Level 7), the most conventional actuators currently used in wind turbines are mechanical flaps/tabs (Johnson et al. 2010; Barlas and van Kuik 2010; Ferreira et al. 2016) (similar to aeronautical accessories). Furthermore, some more innovative concepts based on fluidic and plasma actuators are very promising, since they are devoid of mechanical parts, have a fast response and can be driven in unsteady modes to influence the natural flow instabilities, such as Kelvin–Helmholtz or von Karman ones.

The two papers by Johnson et al. (2010) and Barlas and van Kuik (2010) constitute, to the best of our knowledge, the first state-of-the-art reviews on AFC applied to wind turbine blades. In Johnson et al. (2010), 15 devices were described with respect to their potential for aerodynamic load mitigation. Because the devices presented varying stages of maturity, no attempt was made to compare them and no field tests had been conducted to prove their effectiveness at that time, though the microtab concept was presented as a viable option for AFC. Barlas and van Kuik (2010) also argued that trailing edge flaps were a viable option and gave a wider review of control methods including a discussion of sensors and controllers.

In this context, the present paper aims at giving a state-of-the-art review of current research into wind turbine-oriented flow control strategies applied at the blade scale. It provides an overview on research conducted in the last decade dealing with the actuators and devices devoted to developing AFC on rotor blades, focusing on the flow phenomena that they cause and that can lead to aerodynamic load increase or decrease. It does not go into details about complete AFC systems that include sensors and control methods.

The following two sections provide some general background on wind turbine blade aerodynamics and on the atmospheric flows in which HAWTs operate to keep specific features of HAWT aerodynamics in mind. Section 4 discusses the recent experimental studies on flow separation control and circulation control. It is followed by a discussion about their overall limitations in the wind energy context, with a focus on a few studies that attempt to provide a global efficiency assessment and wind energy-oriented energy balance.

2 Aerodynamic operating conditions of wind turbine blades

When considering how large size classical HAWTs operate, the primary issue is aerodynamics, since the aerodynamic configuration governs the wind turbine (WT) performance as well as the aerodynamic loads which determine the structural sizing of the blades and of all the components.

First, assuming the upstream wind flow as homogeneous and steady, with velocity U_∞, WT blades can be considered, from an aerodynamic point of view, as large aspect ratio lifting systems in rotation. Thus, at first approximation, 2D approaches such as blade element or lifting line are well suited for understanding how they operate. Accordingly, a blade is a set of airfoils along its span. Each airfoil is subjected to a relative incoming flow combining the upstream wind velocity with the rotating motion of the blade. To this relative incoming velocity, a reduced axial flow velocity has to be added together with a rotating flow motion. Both velocity modifications are associated with the effect of the WT on the incoming flow on the blade airfoils (axial and radial induction effects with 3D tip corrections for the blade element momentum theory—3D velocities induced by the wake shed from the blades' airfoil trailing edges and the associated tip vortex for the lifting line theory) (Fig. 1a).

The combination of the axial reduced velocity $U_\infty(1-a)$ with the relative flow velocity associated with the rotor motion and induced flow rotation at blade position r: $-\Omega r\left(1+a'\right)$, with $\lambda = \frac{\Omega R}{U_\infty}$, the WT tip speed ratio, leads to the relative incoming flow velocity $U_{\mathrm{rel}}(r)$ on each airfoil (Fig. 1b). The local airfoil angle of attack: $\alpha(r) = \varphi - \beta$, with $\beta = \beta_{\mathrm{twist}}(r) + \beta_{\mathrm{pitch}}$, where β is the local airfoil angle setting relative to the rotor plane, which is the sum of the twist $\beta_{\mathrm{twist}}(r)$ along the blade and the global WT pitch control β_{pitch}.

U_{rel}, α, a, a' depend on the radial position r of the airfoil on the blade, and the summation of the contribution of each airfoil along the blade results in the aerodynamic performance (torque, power, etc.) and global load on the wind turbine.

As seen in Fig. 1c, most of the airfoil contribution to the blade aerodynamic loads as well as to the WT shaft torque is associated with the lift $L(r)$, the aerodynamic force component perpendicular to the local relative velocity U_{rel}, particularly since pitch-regulated WTs are considered, for which the angle of incidence always remains—under normal working conditions—below stall, and which, at optimum, corresponds to the maximum lift to drag ratio.

Accordingly, lift may be expressed as:

$$L(r) = \frac{1}{2}\rho U_{\mathrm{rel}}^2(r)c(r)C_{\mathrm{L}}(r); \tag{1}$$

in the linear region of the lift versus incidence curve:

$$C_{\mathrm{L}}(r) = C_{\mathrm{L}\alpha}(r)\left(\alpha(r) - \alpha_0(r)\right). \tag{2}$$

Consequently, HAWT aerodynamics may be addressed considering the following parameters:

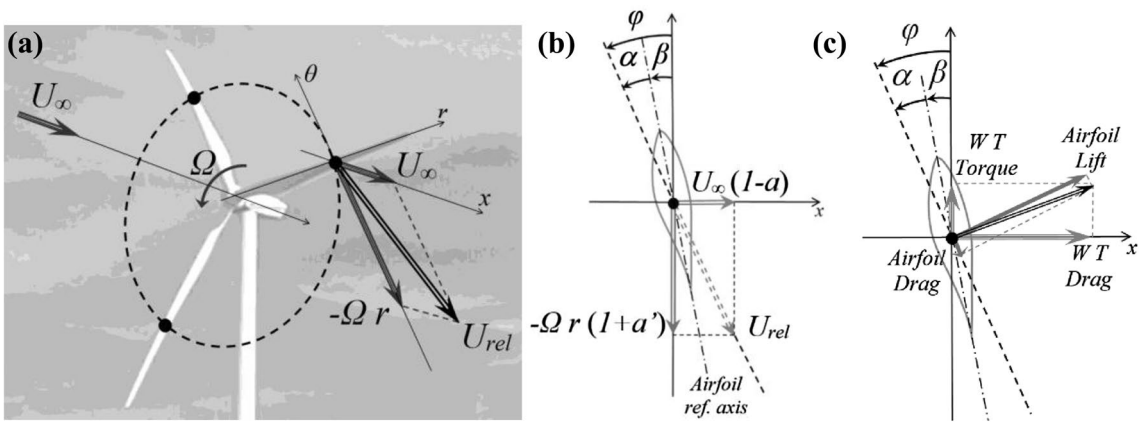

Fig. 1 **a** Velocity diagram of the wind turbine; **b** velocity and **c** force diagrams of an airfoil of the blade

- The number of blades.
- The geometry of the blades: rotor radius R and airfoil characteristics distribution along the blade span (airfoil type, aerodynamic characteristics $C_L(r)$, chord $c(r)$, twist $\beta_{twist}(r)$).
- The tip speed ratio λ through mean wind velocity U_∞ and rotor rotational velocity Ω.
- The pitch setting β_{pitch}.

As far as thickness is considered, stall-regulated WT airfoils are most often rather thick airfoils, with the maximum relative thickness t/c located as far aft as possible (typically, 21% at about 38% of the chord for the classical S809 WT airfoil—Somers 1997), generally for structural reasons (lightness, rigidity) as well as aerodynamic ones (progressive stall lift curve). In the case of pitch-regulated WT, inboard airfoils most generally have high t/c, whereas outboard ones tend to have t/c values lower than 20%. For example, the NREL 5 MW WT is equipped with DU (Delft University) airfoils with t/c varying from 40% at $r/R = 16$–21% at $r/R = 66\%$ approximately, and turning into an NACA one with $t/c = 18\%$ from $r/R = 75.5\%$ (Jonkman et al. 2009).

Once the airfoils' chord distribution along the blade $c(r)$ has been defined, including some structural concerns together with aerodynamic issues related to load distribution on the rotor disc (Schubel and Crossley 2012), the design of the HAWT focuses particularly on the twist angle distribution $\beta_{twist}(r)$. This is done by considering a design tip speed ratio value and an optimum airfoil angle of attack. The optimum angle of attack α_{opt} selected usually corresponds to a lift to drag ratio around the maximum value for performance, which also offers an incidence margin relative to stall, so that the lift coefficient is around 80% of its maximum value (Somers 1997).

This translates into an optimum twist distribution $\beta_{twist}(r)$ which is associated with the specific design tip speed ratio. If the tip speed ratio is not at its design value, then the angle of attack distribution is no longer optimum along the blade, and the performance is decreased.

An additional parameter has to be mentioned: the Reynolds number, $Re = \frac{U_{rel}\, c(r)}{\nu}$, which varies along the blade span with the radial position, depending on the blade geometry and the kinematic conditions U_∞ and Ω. Its main effect is on the airfoil aerodynamic lift performance, which may be strongly downgraded at low Re values. It means low values of U_∞ and/or Ω and/or radial position r, especially at high C_L values and at stall (stall angle of attack, maximum lift coefficient) (Somers 1997).

As the loads on the HAWT result from the added contributions of each airfoil along the blade, from the structural point of view, the aerodynamic load distribution on the blades induces efforts in the blade structure, one of the most important of which is the bending moment along the blade, which is maximum at the blade root, not forgetting the chord-wise torsion moment

Once the aerodynamic design has been finalized, power production will depend on the upstream wind velocity. Classical large-scale HAWT power curves show four regions (Johnson et al. 2008):

In region I, wind velocity is too low to allow the HAWT to start. In region 2 (sub-rated power region), the wind has reached a high enough velocity to start the wind turbine, and power production increases according to the cubic dependency of the collected power on the wind velocity. In region III, power reaches the rated power and is kept constant by means of the wind turbine regulation system. Region IV corresponds to the wind turbine shutdown at such high wind velocities that the WT could be damaged or even destroyed.

Focusing on regions II and III, large modern HAWTs operate with a variable rotor rotational velocity Ω together with collective pitch control β_{pitch}. In region II, rotor velocity increases with wind velocity so that HAWTs operate at their design tip speed ratio, with optimum working conditions up to the rated power. In region III, blade collective pitch is set so that the rotor operates at constant torque with a constant rotational speed Ω, such that power output is kept constant (rated power) whatever the wind velocity, up to shutdown. One drawback associated with the low t/c values for outboard airfoils is blade flexibility, both spanwise bending and chordwise twisting, making blade pitch less controlled along the blade.

Performance improvements in region II, where the HAWT operates at the design tip speed ratio, concern improving airfoil aerodynamic performance at low Re, allowing the wind turbine to start at lower wind speed and provide improved performance at low wind velocity. In region III, performance is voluntarily reduced relative to the design tip speed ratio by means of pitch control.

3 Wind turbines are aerodynamic systems immersed in atmospheric flows

Wind velocity is neither spatially nor temporally constant. WTs are therefore aerodynamic systems immersed in atmospheric flows. The approach flow is strongly inhomogeneous in the vertical direction, following a power law whose exponent is directly dependent on the type of terrain (Fig. 3a). For example, the wind speed gradient through the rotor ranges from 1.5% above slightly rough terrain such as offshore conditions to 5% above very rough terrain such as forest canopies (under neutral stability conditions). Additionally, the approach flow is highly turbulent, with a streamwise turbulence intensity ranging from 5 to 30% (Fig. 3b) (Kaimal and Finnigan 1994; ESDU 1985; Counihan 1975). Wind conditions are also driven by the thermal stability of

the atmosphere, leading to even more scattered operating configurations. Unlike aeronautical applications, the relative velocity encountered by the wind turbine blades is not significantly higher than the wind speed; therefore, its properties are not negligible compared to the blade moving speed.

As an example, a typical 3 MW turbine has a rotor radius R of 50 m and a hub height of 90 m. It reaches its rated power (region III in Fig. 2) when the wind speed at hub height U_{hub} is around 13 m/s and its rotor speed Ω is 1 rad s^{-1} (one revolution in 6 s), leading to a shear time scale $T_s \approx 6$ s. Due to the wind speed gradient on the vertical dimension, the blade encounters 6 s periodic wind speed fluctuations of ± 5 to $\pm 14\%$ (derived from Fig. 3a) and, so, the geometric angle of attack fluctuations of ± 5 to $\pm 10\%$ at a radius of $R_d = 3/4\ R$ (typical location where the maximum loads are generated), leading to periodic flapwise bending moment fluctuations at the blade root of ± 10 to $\pm 40\%$, depending on the terrain (Burton et al. 2001; Sathe et al. 2013).

Atmospheric turbulence generates additional 3D wind speed fluctuations of the same order of magnitude, but the associated time scales are broadband and non-deterministic, from tenths of seconds to several minutes, centered on the most energetic eddy-related time scale from around $T_t \approx 3$–15 s, depending on the terrain. Traditionally, the velocity statistics due to atmospheric turbulence are represented with a Gaussian probability distribution, which is expected to be acceptable up to $\pm 3\sigma$, with σ the standard deviation of the statistics (Counihan 1975). Beyond these limits, it has been proven that the turbulence has an anomalous distribution due to the intermittency of turbulence (Peinke et al. 2004). This is illustrated by a higher probability of occurrence of short-time or small-scale wind gusts, called *extreme events*. As a result of the strong coupling between the inflow turbulence and the HAWT response, the intermittency of atmospheric turbulence can be observed in the wind turbine aerodynamic load fluctuation distributions (Mücke et al. 2010). This means that the nature of the turbulence should be taken into account as a particular source of disturbance during the control system identification.

Both sources of fluctuations, the periodic one due to shear and the non-deterministic one due to turbulence, are superimposed on the local inflow conditions of the blade and their individual effects cannot be easily identified. On the other hand, with a classical blade chord of 2 m (at the radius R_d), the typical time scales of both fluctuations are at least 100 times higher than the typical chord time scale $T_c \approx 40$ ms, leading to an almost steady-state problem from the aerodynamic point of view and hence for the control strategies used to mitigate these fluctuations (nevertheless, dynamic stall, characterized by time scales of the order of magnitude of the chord time scale must be taken into account during blade design).

These spatial and temporal wind fluctuations can have two kinds of effects on WT operation:

- Fluctuations around nominal loads inducing fatigue of the blade structure, when pitch regulation is either not efficient enough, or too complicated or challenging to achieve.
- Extreme loads, above nominal ones, in the event of a rapid wind velocity increase, when pitch regulation is too slow to be able to avoid them, and the stall margin together with dynamic stall hysteresis are unable to

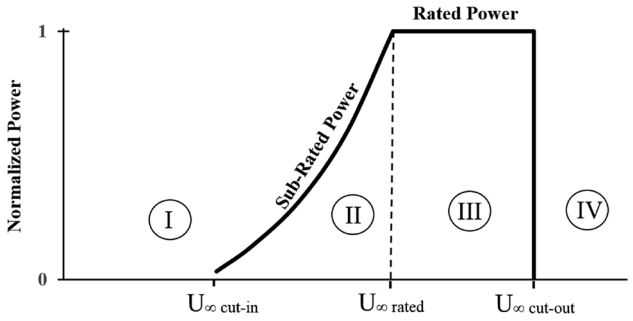

Fig. 2 Typical power curve showing the operating regions

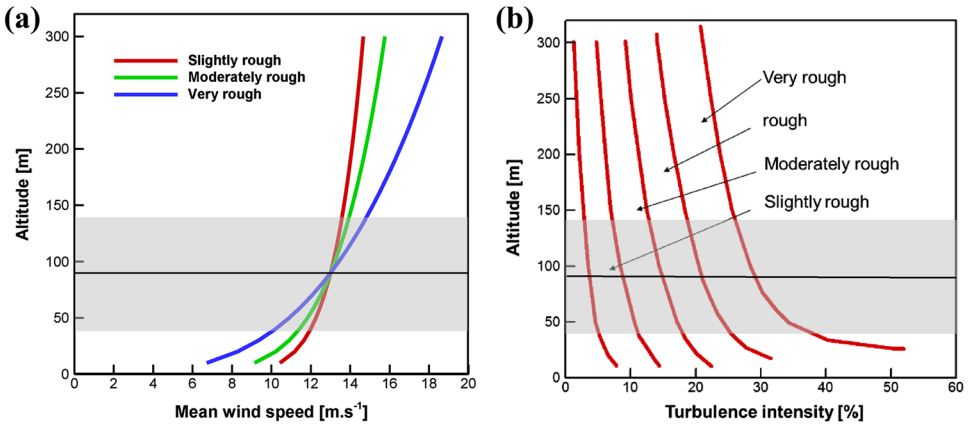

Fig. 3 **a** Typical mean wind speed and **b** turbulence intensity profiles for different terrains under neutral stability conditions. Wind speed profiles are designed to reach a typical nominal wind speed of 13 m s^{-1} at a hub height of 90 m. *Gray shaded areas* show the rotor location. *Black lines* show the hub height

reduce aerodynamic loads by means of stall. This may increase structural loads above what is acceptable by the structure, or require an oversizing of the blade structure to be able to resist such loads, associated with higher structural mass, cost, etc.

4 Wind energy-oriented flow control strategies

From this brief analysis of the aerodynamics of large HAWTs and its effects on performance and structural loads, it is clear that air flow control on wind turbine blades may be valuable to tackle three issues. The first one is improving the low wind velocity behavior of the HAWT to improve performance. The second is reducing the load fluctuations and induced structural fatigue at nominal working conditions, with a view to reducing maintenance requirements and thus increasing the reliability of the wind turbine. The last one is reducing the extreme loads associated with high wind velocities, leading to blade mass and cost reduction.

Depending on the issue concerned, distinct flow control strategies will be considered. When the working lift is set to its optimal operating value (usually 80% of the maximum lift obtained with this blade section, Burton et al. 2001), the flow is fully attached to the blade. The inflow velocity fluctuations may generate relative velocity fluctuations at the blade, in magnitude and direction. The lift fluctuates around the working lift, but without reaching the maximum lift before stall. Aerodynamic load fluctuations are therefore generated. A control strategy focusing on alleviating these fluctuations is possible and would be based on the control of circulation, which is made possible by placing actuators at the trailing edge of the blade section. Despite this precaution on the design limit of 80% and in the event of very high inflow velocity fluctuations, the stall angle could be reached, leading to strongly deteriorated aerodynamic performance, magnified by the presence of a hysteresis on the angle of attack to reattach the flow that makes the return to the optimal working lift configuration difficult to obtain. In this configuration, circulation control becomes inappropriate, whereas separation control would be suitable. Ideally, this type of control requires arranging distributed actuators all over the suction side of the blade. However, separation control can be advantageously developed for different purposes as load mitigation during nominal operation, active stall regulation (in areas where the noise impact is not essential) and improving the start-up process, when the local angle of attack is very high.

The non-deterministic nature of the turbulence forces the control strategy to be based on a feedback loop, reacting to a detected disturbance. Having access to the incoming flow properties in real time means that this information can be taken into account in the control loop, leading to a predictive control strategy (Schlipf and Kühn 2013). This is made possible thanks to new LiDAR measurement systems mounted on the wind turbine nacelle that measure in quasi real time the incoming flow fluctuations at a distance from 30 to 150 m upstream of the wind turbine rotor (Wagner et al. 2014). Even if this system encounters limitations due to the inhomogeneity of the turbulent flow and its constant evolution during advection, it widens the scope of possibilities in terms of control opportunities.

4.1 Flow separation control

As mentioned earlier, flow separation and aerodynamic stall appear on the suction side of wind turbine blades even if they are designed to prevent this configuration. These phenomena mainly occur during the start-up process, when the pitch angle of blades cannot be appropriate for the whole span and when the effective velocity and angle of attacks change to reach the nominal rotor velocity rotation. The separation process can be characterized by time scales that are rather short in comparison to the airfoil time scale, inducing dynamic stall. Additionally, the high-level turbulence intensity in the freestream flow is also a source of intermittent stall periods on critical blade parts. Associated time scales can generate dynamic stall for the shorter ones and quasi-static stall for the higher ones. This leads to a performance loss and can generate additional load fluctuations. These situations justify the need to study the AFC on partially to massively separated flows on wind turbine blades, for steady and unsteady flow configurations.

In the literature, all actuator technologies are used but with a predominance of fluidic (Ekaterinaris 2004; Maldonado et al. 2010; Stalnov et al. 2010; Wang et al. 2011; Shun and Ahmed 2012; Troshin and Seifert 2013; Chawla et al. 2014; Niether et al. 2015; Xu et al. 2016) and plasma actuators (Nelson et al. 2008; Meijerink and Hoeijmakers 2011; Walker and Segawa 2012; Greenblatt et al. 2012; Greenblatt and Lautman 2015; Ben-Harav and Greenblatt 2016; Brownstein et al. 2014; Jukes 2015). Action strategies are mainly driven by the capacity to generate 3D longitudinal vortices in the boundary layer as close as possible to the separation point, to promote the transfer of high momentum flow toward the wall and to delay, or suppress, the separation. Consequently, actuators are designed to act as vortex generators (VGs). Given the dependence of the separation location on the wind conditions (wind speed and angle of attack), no universal actuator location on the airfoils exists. Studies are therefore performed with a fixed actuator location (Maldonado et al. 2010; Stalnov et al. 2010; Wang et al. 2011), or with a finite number of locations distributed all over the suction side, working separately or simultaneously (Nelson et al. 2008; Meijerink and Hoeijmakers 2011; Troshin and Seifert 2013; Chawla et al. 2014).

The intensity of action can be transposed as a momentum coefficient c_μ for plasma and fluidic actuators (Cattafesta and Sheplak 2011). It indicates the ratio between the momentum supplied by the actuator and a reference momentum. For airfoil configurations, it is classically written as:

$$c_\mu = \frac{T}{\frac{1}{2}\rho U_\infty^2 . A_{\text{airfoil}}}, \tag{3}$$

$$c_\mu = \frac{\dot{m}_{\text{inj}} v_{\text{inj}}}{\frac{1}{2}\rho U_\infty^2 . A_{\text{airfoil}}}. \tag{4}$$

Equation (3) is used for plasma actuators, where T is the global thrust force supplied by the plasma actuator to the local flow and characterized by an "ionic" wind, similar to a wall jet in quiescent air. This force can be deduced by the momentum theory applied to the wall jet (Meijerink and Hoeijmakers 2011). The power consumption can be directly measured through the electrical circuit supply (Brownstein et al. 2014). Equation (4) is used for fluidic actuators, where $\dot{m}_{\text{inj}}$ is the injected mass flow rate and v_{inj} the injection velocity.

Both types of actuators can work continuously (in comparison to the airfoil time scale) or with an unsteady mode. In that case, the acting frequency is reduced by the airfoil time scale, which corresponds to the ratio between the chord length and the upstream reference velocity. Various studies have shown that the acting frequency can play a role on the control efficiency but that it is not the primary parameter. On the other hand, having some acting reduced frequencies lower than 1 could generate some strong load fluctuations that would be of damage for blade fatigue (Ekaterinaris 2004). Gross and Fasel (2012) applied AFC to control a laminar separation bubble on the suction side. In that case, the frequency was a key parameter since the physical mechanism responsible for the control efficiency was the excitation of the natural instabilities of the laminar boundary layer.

For 2D configurations, the control authority indicator is the gain or loss in lift coefficient compared to the baseline case ΔC_L. In the cases where the objective is to delay the separation, and so to delay the stall for higher angles of attack, a gain of $\Delta C_L \approx 0.1-0.3$ can be achieved in the upper part of the lift curve, which is a promising result, according to the authors. Additionally, Niether et al. (2015) applied a spatially optimized continuous action with blowing jets on a 2D airfoil to smooth out the lift curve close to the stall region and they were able to reduce lift fluctuations by one order of magnitude in cases of incursions to stall regime due to external conditions. Wang et al. (2011) reduced lift fluctuations by 12% with a closed-loop control of blowing jets for a 2D airfoil with the presence of large-scale unsteadiness in the freestream flow.

This variation of $\Delta C_L \approx 0.1-0.2$ is definitely unsatisfactory if one plans to use AFC to replace standard pitch regulation by an active stall regulation. Pereira et al. (2014) showed that this objective would require generating a lift reduction of up to $\Delta C_L \approx 0.7$, whereas they were able to reach 0.3–0.4. Indeed, a notable feature of their study is that they extrapolated experimental results obtained on a 2D airfoil to a HAWT configuration, using the blade element momentum (BEM) method to determine the potentialities of this type of control on a full-scale rotating machine.

Jukes (2015) studied two plasma flow control strategies on a two-blade rotating HAWT model (Fig. 4). He compared the efficiency of co-flow and VG-type plasma actuators for reducing the drag coefficient, deduced from the integration of the velocity deficit in the blade wakes. He showed that the radial body forces generated by plasma VGs are of paramount importance in rotating separated flows.

Two full-scale experiments with plasma actuators are worth mentioning. The first one was performed on a 10 m-diameter HAWT using DBD actuators located at the

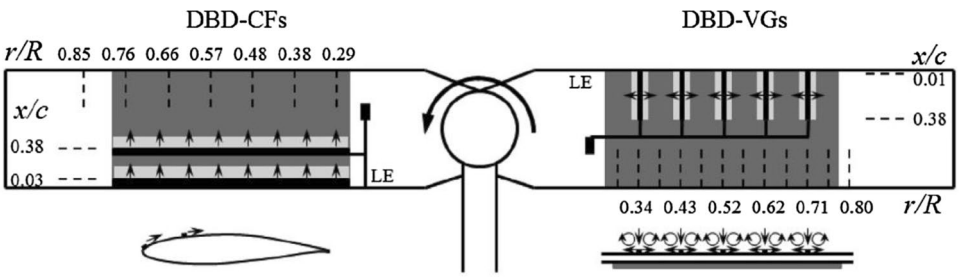

Fig. 4 Schematic view of HAWT from downstream. Co-flow plasma actuators on left hand blade (DBD-CFs). Plasma vortex generators on right hand blade (DBD-VGs). Plasma forms in the *light gray* region adjacent to the *thick black upper* electrodes, with forcing direction indicated by *arrows*. *Lower* schematics show operating principles Reprinted from Jukes (2015), original figure 4; with permission from Elsevier

leading edge and along 4 m of span (Tanaka et al. 2013). The increase in production during plasma activity was shown to be at least three times higher than the actuator power supply. The second one was performed on a 20 kW HAWT (9.5 m in diameter), using actuators located at mid-chord or close to the trailing edge on the suction side (Cooney et al. 2016, Fig. 5). A power gain from 2 to 6% depending on the operating points was observed, even if the limited operating lifetime of the actuators prevented reaching converged datasets.

Studies about AFC of dynamic stall are often related to vertical axis wind turbines (VAWT), where the rotation axis normal to the wind direction leads to even more complex flow unsteadiness. Greenblatt et al. (2012), Greenblatt and Lautman (2015) and Ben-Harav and Greenblatt (2016) applied DBD plasma actuators at the leading edge of a laboratory-scale VAWT and reported that an increase in gain of 38% could be reached for a power supply delivered to plasma actuators of a few percent.

Maldonado et al. (2010) and Wang et al. (2011) have proposed closed-loop control strategies. Both developed simple controllers with the aim of reducing load fluctuations during large-scale unsteadiness. The first one targeted the minimization of the root strain spectrum (3D finite span translating airfoil), whereas the second one targeted the minimization of the pressure fluctuations at the leading edge (2D translating airfoil). Both showed the ability to significantly reduce load fluctuations, but these strategies were not further developed in subsequent publications.

Troshin and Seifert (2013) showed the benefit of a closed-loop control with synthetic jets distributed on the suction side to recover the decrease performance due to degraded surface quality.

4.2 Circulation control

As mentioned above, mitigation of load fluctuations on HAWT rotor blades, also known as load alleviation, most generally refers to reducing the magnitude of the fluctuations of the bending moment on the blade where it is at its maximum, i.e., at the root, to reduce fatigue loads on this critical part, and thus extend lifespan. Therefore, as this bending moment mainly comes from the lift distribution on the blade airfoils, the lift on some part of the blade has to be either increased or reduced by means of an AFC device without changing the incidence on the airfoils.

It has also been noted that, for large-scale HAWTs, blade airfoils operate with some incidence margin relative to stall and this requires the aerofoils equipped with AFC devices to operate in the linear part of the C_L vs incidence curve. Therefore, this lift control belongs to the generic issue known as "circulation control" (CC), which refers to the relation between the aerofoil lift and the velocity circulation around it. As far as the amplitudes of C_L variations required

Fig. 5 Renewegy VP-20 wind turbine with retrofit plasma actuators on the blade's suction side Original figure 26 reproduced from Cooney et al. (2016); reprinted by permission of the American Institute of Aeronautics and Astronautics, Inc

for load alleviation on large HAWT are concerned, Cooney (2009) mentions, on a simple computational basis, that variations around ±0.1 or 0.2 are suitable. Holst et al. (2015), who simulated the NREL 5 MW large HAWT subjected to inflow fluctuations with the FAST aerodynamic/aeroelastic tool, provided realistic time series of lift fluctuations showing the variance of the lift coefficient to be of the order of $\Delta C_L = \pm 0.2$. Thus, the order of magnitude of C_L variations of ±0.1 or ±0.2 is commonly considered as a satisfactory target for AFC devices efficiency.

Looking at the literature, most of the references deal with 2D airfoil laboratory implementations (and computations) of AFC actuators. One can also find some 2D laboratory closed-loop lift control applications. In this case, the HAWT blade load alleviation problem is replaced by a simpler alternative one which consists in subjecting a 2D aerofoil to load fluctuations, essentially by means of velocity variations, and developing AFC techniques—including actuator and closed-loop control—to keep lift as constant as possible. Concerning devices for circulation control around an aerofoil, two kinds of technologies are encountered: mechanical and fluidic. Mechanical systems were the first to be introduced and were generally developed for aeronautical applications, and not specifically for HAWT, but are now the most widespread techniques. The first can be mentioned as the plain flap which has been considered in the case of HAWT (Berg et al. 2007), a modern variant of which is the flexible flap (Pechlivanoglou et al. 2010). It rapidly appeared that smaller and lighter devices could be of interest for HAWT applications, such as Gurney flaps (GF) or microtabs, which are small fixed or deployable surfaces located near or at the trailing edge (TE) and extending perpendicularly to the airfoil surface. Cooperman et al. (2014) and Cooperman and van Dam (2015) considered a set of deployable tabs (Fig. 6) and

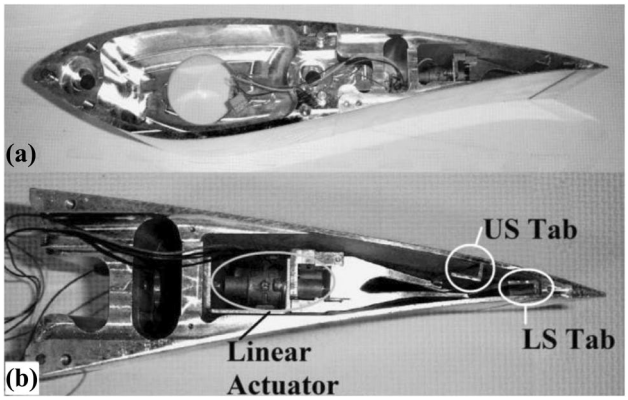

Fig. 6 Spanwise section of the S819 m model with linearly actuated microtabs: **a** full airfoil profile, **b** detached aft section Original figure 1 reproduced from Cooperman et al. (2014)

obtained ΔC_L values between 0.18 and 0.19. They presented the results of an experimental 2D constant lift closed-loop system based on this technology, showing a reduction of the deviation from the desired value of lift by 70–80% on an airfoil subjected to air speed changes.

Nikoueeyan et al. (2014a, b) studied the effects of deployable GFs on a thick TE and showed very good efficiency, exhibiting a ΔC_L value between 0.5 and 0.7 (Fig. 7). Holst et al. (2015) investigated the flow associated with a finite width GF, displaying the 3D effects. They applied their experimental results to HAWT simulations and were able to show a reduction of load fluctuations in the case of large HAWTs and power control without pitch in the case of small ones.

Fluidic systems are also of interest in CC applications. Two possibilities exist: one is associated with an angular TE airfoil and the fluidic AFC device acts as a "virtual flap", and the other one is associated with a rounded TE, and makes use of the Coanda effect to deflect the flow at the trailing edge and generate CC. Cooperman et al. (2014) compared computed blowing jets on a 2D configuration with the microtabs presented above, and simulated in this case a 2D constant lift control system. They achieved ΔC_L values comparable with those obtained with the microtabs presented above (Fig. 8), but do not mention the corresponding c_μ value. De Vries et al. (2014) investigated experimentally and numerically the effects of a synthetic jet perpendicular to the surface of an airfoil near the TE. The experimental setup did not allow high enough frequencies to have significant effects, but computations indicated ΔC_L of the order of 0.2 with reduced frequency F^+=20 ($F^+ = \frac{f_j c}{U_\infty}$, where f_j is the synthetic jet frequency, c the airfoil chord and U_∞, the incoming flow velocity).

Circulation control using the Coanda effect on rounded TE has generated a great number of studies with aeronautical applications in mind. A recent work has revealed renewed attention. Wetzel et al. (2013) showed the interest of such a system with blowing jets on a rounded TE for underwater applications. In the case of wind turbine applications, Braud and Guilmineau (2016) developed a distributed blowing jet array that generates 3D effects on a rounded TE which proved experimentally and numerically efficient (ΔC_L maximum of 0.25 at 8° of incidence with a momentum coefficient $c_\mu = 0.049$; see Eq. (4)).

Together with classical blowing or synthetic jet fluidic actuators, the development of plasma technologies in flow applications with dielectric barrier discharge (DBD)

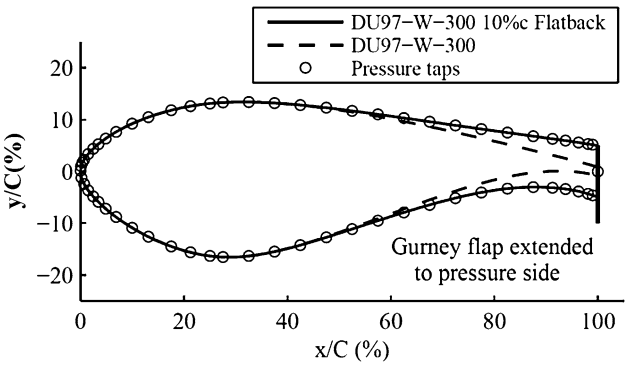

Fig. 7 The original DU97-W-300 airfoil and the 10%c thick trailing edge flatback airfoil Original figure 2 reproduced from Nikoueeyan et al. (2014b); reprinted by permission of the American Institute of Aeronautics and Astronautics, Inc

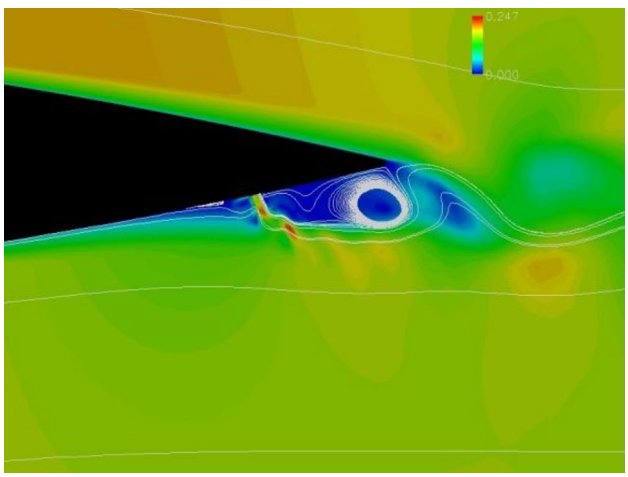

Fig. 8 OVERFLOW simulation showing the flow velocity and instantaneous streak lines around an airfoil with an activated pressure side jet, $\alpha = 0°$, $Re = 1.0 \times 10^6$ Original figure 2 reproduced from Cooperman et al. (2014)

plasma actuators has allowed their application to circulation control. Nelson et al. (2008) and Cooney (2009), in addition to the stall delay mentioned in the previous section, developed a CC strategy. A DBD near the angular TE of an S827 airfoil allowed them to obtain an average lift coefficient increase of 0.075. The effect of plasma actuation is presented as equivalent to increasing the camber of the airfoil, and they point out that the potential of the approach is in using multiple plasma actuators at different *x/c* locations, combining their effect.

Kotsonis et al. (2014) used a DBD actuator on a rounded TE. Though at rather low Reynolds number values (1.4×10^5–2.8×10^5), their experiments showed a ΔC_L of about 0.1. They also analyzed the effect of the position of the DBD, and its effect on the wake flow field. Baleriola et al. (2016) also used a DBD actuator on a rounded TE and showed (Fig. 9) that it was possible to achieve positive and negative lift variations (ΔC_L of about ± 0.08) with two dedicated sets of multi DBD plasma actuators. Because of the electrical nature of the surface plasma actuation, the tangential jet remains attached to the wall and follows its curvature in a more efficient way than a jet subjected to the Coanda effect (Fig. 9). Lastly, Feng et al. (2012) combined GF and plasma actuation at low Reynolds number and showed that the two effects added together, with a GF effect on ΔC_L of about 0.5, while plasma actuation on the GF added an extra ΔC_L of about 0.2.

At the WT scale, a certain number of numerical simulations of HAWT behavior submitted to simulated incoming turbulence are reported. They make very generally the use of 2D experimental or computational results for the airfoil behavior with AFC in a 3D approach based on BEM or lifting line with free vortex wakes. An example is Zhang et al. (2014), who developed an aero-servo-elastic model based on FAST/Aerodyn and Matlab/Simulink software. They simulated the NREL 5 MW HAWT equipped with a "smart rotor control" including a torque generator and collective pitch controller, with deformable TE flaps on the blades controlled independently by a feedback loop method. Results showed in particular that, under the IEC extreme wind shear condition and compared with the original collective pitch control method, the extreme load on blades was effectively reduced. The maximum reductions in the flapwise root moment and the tip deflection of blades were up to 43.1 and 40.1%, respectively.

Very recently, an example of a complete 3D HAWT computation was presented by Chen and Qin (2017). A 3D RANS computation in the rotational framework of the NREL Phase VI blade was compared with wind tunnel experimental data. This computation included TE flow control microtabs and microjets together with a divergent trailing edge as a passive flow control device. The results appear very interesting, demonstrating that deploying TE flow control devices can effectively improve the power output of a stall regulated wind turbine, and above all, the possibility of taking AFC into account in a real 3D numerical approach.

The literature reveals very few experimental HAWT controls for load alleviation, either in the laboratory or on site field tests. Nevertheless, the collaborative efforts on AFC via trailing edge flaps on a small research wind turbine in the TU Berlin large wind tunnel facility reported in Vey et al. (2015) and the work by Berg et al. (2014) at Sandia may be mentioned . In this study, a WT rotor with TE flaps has been developed and field tested. Results show the control capability of the TE flaps, the combined structural and aerodynamic damping and direct observation of time delays associated with aerodynamic response. Nevertheless, no practical load alleviation has yet been reported.

5 Discussion

Table 1 in the Appendix summarizes the main experimental studies related to AFC for wind energy applications that are cited here. From the present review, some general conclusions can be drawn regarding the relevance of the aerodynamic configurations and of the efficiency assessment of AFC.

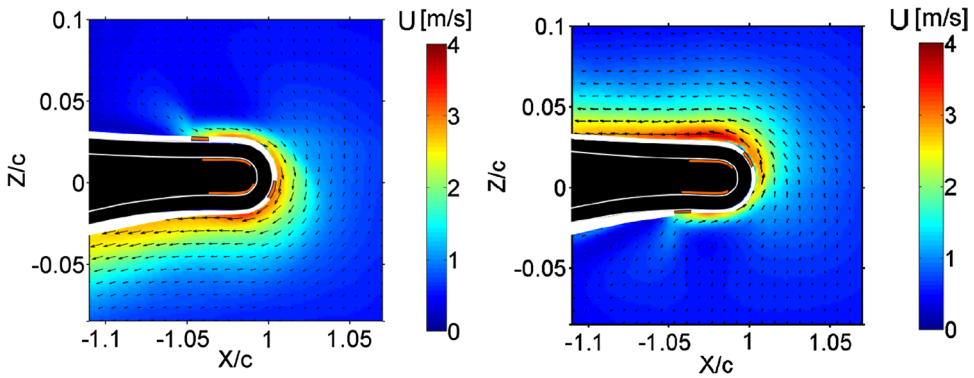

Fig. 9 Time-averaged magnitude velocity field and vector fields of the flow induced under quiescent air conditions by plasma actuators located at the rounded trailing edge of a circulation control-oriented airfoil and acting toward the pressure side (*left*) and toward the suction side (*right*). Electrodes are represented in *orange* Original figure 8 reproduced from Baleriola et al. (2016)

5.1 Aerodynamic configurations

A HAWT is composed of rotating blades, but only a few authors study this problem with a 3D rotating configuration, but rather choose a 2D translating configuration. This is justified by the fact that it is particularly complex to embed some actuators and sensors in a rotating body (particularly at laboratory scale), and that the measurement diagnostics are often reduced to more global information such as rotor torque and extracted power. Even if the latter are crucial for wind energy applications and are used as final indicators of control efficiency, they are not sufficient to interpret the strongly 3D aerodynamic phenomena taking place on the rotating blades. Moreover, reducing the configuration to a 2D problem leads to totally neglecting the 3D properties of the separation area on a rotating body, due to centrifugal forces. Indeed, the reverse flow on the suction side of blades has a component along the span toward the tip that modifies the overall pressure distribution. This simplification from 3D to 2D is less critical when the flow is attached since the 3D study can be reasonably modeled by a combination of successive 2D configurations along the span.

The Reynolds number similarity is also a recurrent issue. Most investigations are performed through wind tunnel experiments or numerical simulations for Reynolds numbers based on the chord of $O(10^5)$, whereas modern wind turbines reach $O(10^6–10^7)$. This has two main consequences:

- It might be necessary to trip the transition on the tested airfoils to prevent the transition to the turbulent boundary layer from occurring in the wrong place and the presence of laminar bubble separation.
- Even if the transition is triggered, the drag coefficient is strongly dependent on the Reynolds number (unlike the lift coefficient), meaning that the consequences of the AFC on both aerodynamic loads cannot be fully extrapolated to higher Reynolds number configurations.

The freestream turbulence effects on the flow control efficiency are also totally ignored in wind tunnel experiments. This can be justified by the fact that the most energy-containing turbulent eddies in the atmosphere are 1000 times larger than the boundary layer thickness on blades, but residual turbulence at smaller length scales might have an effect on the different flow control processes.

Bearing all these limitations in mind, studies on 2D translating airfoils in low-turbulent flows remain indispensable and an essential step on the way toward more realistic, and hence more complex configurations.

5.2 Efficiency assessment of active flow control and wind energy-oriented energy balance

After 40 years of research in the field of AFC, and considerable relevant research in aerospace applications, some important questions remain unanswered:

- The upscaling of innovative control strategies developed at small scales to the full scale is still challenging. Both papers (Tanaka et al. 2013; Cooney 2009) illustrate the technical problems encountered in performing robust actuator integration and reliable field measurements. Despite promising outcomes, it remains difficult to assess AFC benefits. To our knowledge, further literature showing convincingly the efficiency of AFC on real-scale research or industrial demonstrators is required. Moreover, the physical mechanisms and their key scales are not fully identified and cannot be extrapolated to other scales. In other words, the similarity laws of the actuators still need to be studied.
- The wide variety of actuators and configurations that are studied makes the identification of the most efficient actuators with respect to the tested configurations and flow regimes almost impossible. If the energy capture is targeted, an extensive analysis of the action efficiency, based on an (wind energy oriented or not) energy balance between the supplied and the gained energy with several actuator types according to a class of given geometries and to pre-defined objectives still needs to be performed. If load mitigation is targeted, the efficiency assessment becomes more delicate since it refers to more elaborated metrics coupling aerodynamic and structural behaviors. The action efficiency should be quantified according to weight loss and/or WT life duration increase due to fatigue load reduction.

It is worth mentioning the definition of a wind turbine-oriented Aerodynamic Figure of Merit AFM3 by Stalnov et al. (2010) to evaluate the overall system efficiency by considering the ratio between the generated power, with and without AFC during the HAWT start-up process (assuming $\varphi \approx 45°$, common angles during start-up conditions):

$$\mathrm{AFM3} = \frac{\left[(L-D)U_{\mathrm{eff}}\right]_{\mathrm{controlled}} - 2P_{\mathrm{elect}}}{\left[(L-D)U_{\mathrm{eff}}\right]_{\mathrm{baseline}}}, \tag{5}$$

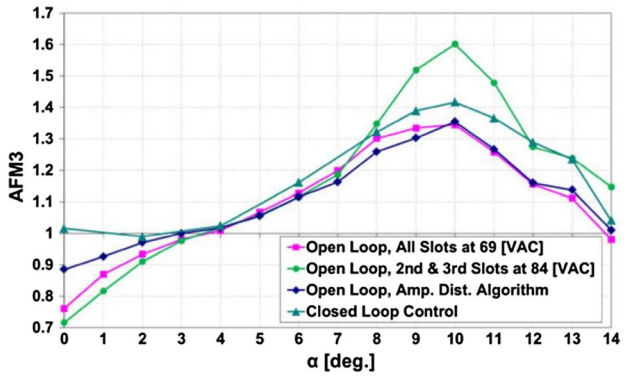

Fig. 10 Wind turbine-oriented Aerodynamic Figure of Merit AFM3 vs the angle of attack for different strategies of AFC using synthetic jet arrays distributed on the suction side of a thick airfoil with degraded surface quality. The effect of excitation by three actuator rows on lift in four cases: (1) open loop, all slots at constant amplitude; (2) open loop, with slots 2 and 3 at constant amplitude; (3) open loop, with amplitudes distributed automatically based on separation location; (4) closed-loop lift control. $Re = 0.5\ 10^6$ Original figure 20 reproduced from Troshin and Seifert (2013) with permission of Springer

where L and D are the lift and drag components of the aerodynamic force projected in the wind turbine's rotation plane, respectively. U_{eff} refers to the effective freestream velocity. P_{elect} is the power provided to the actuators. The subscript baseline refers to uncontrolled conditions. This type of figure of merit is a first step toward a better assessment of actuator efficiency in a specific sector of applications as demonstrated in Troshin and Seifert (2013) and illustrated in Fig. 10. Indeed, AFM3 is used to assess different control strategies performed to recover aerodynamic performances for wind turbine thick airfoils with degraded surface quality over an incidence range. Values of AFM3 greater than 1 indicate an energy benefit provided by AFC.

In Barlas and Van Kuik (2010), aerodynamic device concepts were compared in terms of lift control capability; see Fig. 11. In the same vein, Pechlivanoglou (2013) attempted to estimate the overall performance of 14 actuators in various technical fields that are relevant for the wind energy sector (Fig. 12), including wider features such as blade implementation, cost or operation capabilities.

6 Summary and future trends

The wind energy sector gives rise to aerodynamic issues that the active flow control scientific community has identified as challenges to take up. Through the present review, it has been shown that the motivations for applying AFC on wind turbine blades are various and require non-universal AFC strategies, leading to the conclusion that the future developments are probably in the development of spatially distributed actuation.

The AFC research dedicated to wind energy was initially characterized by a transfer of knowledge from aeronautical to wind energy applications, whereas the interactions between both communities are now better balanced. The fundamentals of fluid dynamics are identical, but this trend also generates some limitations since the actual operating

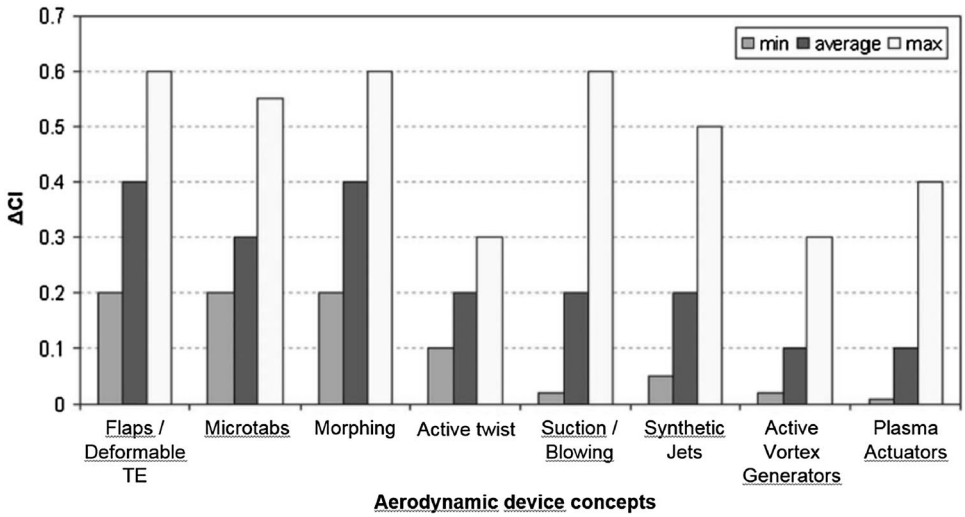

Fig. 11 Comparison of aerodynamic device concepts in terms of lift control capability Original figure 9 reproduced from Barlas and van Kuik (2010) with permission from Elsevier

Element selection matrix

Element	Aerodynamics	Mechanics	Blade Integration	Operation	Cost	SUM
VGs & Vortilons	2.0	4.5	5.0	4.0	5.0	20.5
Slat	4.0	4.5	4.5	4.5	3.5	21.5
Flow Vane	4.5	4.5	5.0	3.5	3.0	20.5
L.E. protuberances	2.5	4.0	5.0	3.5	4.5	19.5
Gurney Flap	3.0	4.0	4.5	4.0	4.0	19.5
Rigid T.E. Flap	4.0	5.0	4.0	4.0	3.0	20.0
Flexible T.E. Flap	4.5	2.0	4.5	3.5	4.0	17.5
Flexible L.E. flap	4.5	3.0	2.0	4.5	4.0	18.0
Multi-element Flap	4.0	2	4.5	2.0	2.0	14.5
Split Flap	4.5	4.0	4.0	4.0	2.5	19.0
Stall Ribs	3.5	4.5	4.0	3.0	4.0	19.0
Spoilers	3.0	3.0	2.0	2.0	2.0	12.0
BL Suction & Blowing	4.0	2.0	2.0	2.0	1.0	11.0
Zero Mass Flux	3.5	4.0	3.5	4.0	4.0	19.0
Plasma Actuators	3.0	5.0	4.5	2.0	3.0	17.5

Fig. 12 Estimation of the overall performance of 14 actuators in different technical fields Table reproduced from Pechlivanoglou (2013), page 111. Courtesy of Pechlivanoglou

conditions of wind turbines are seldom taken into account in the studies. A gap between the AFC performance under controlled boundary conditions at laboratory scale and under atmospheric conditions at full scale is indeed observed. It leads to difficulties in evaluating convincingly the outcomes and up to now prevents reaching the Technology Readiness Level 7 (system prototype demonstration in operational environment). This is in fact a general criticism that can be applied to most AFC applications that generally stay at a level described as promising, but rarely reach an industrial level of integration (see Crowther et al. (2010) for a provocative article about flow control fallacies).

While the overall scientific interest of studying AFC effects on flows is not questioned, its applicability to engineering domains will remain uncertain if future studies do not provide better proof of their efficiency in real operating conditions. This depends on several objectives that need to be developed in the future:

- In collaboration with industry, better identify the wind energy-oriented targets of AFC that are priorities (improve performance under nominal operating conditions, improve the start-up process, alleviate loads, etc.) and the metrics to quantify its capacity to reach the objectives in a completely integrated process.
- From a technological point of view, make a joint effort for transdisciplinary studies to develop more mature active flow controllers, in terms of durability, compactness, controllability and integration into wind turbine dedicated industrial products.
- Develop studies on the upscaling issue to reduce the gap between more promising results obtained at the laboratory scale than at full scale.

If these preliminary steps are accomplished, wind turbine-oriented active flow control could finally play a role in the design process of wind turbines.

Appendix

See Table 1.

Table 1 Summary of the main cited experimental works related to active flow control and dedicated to wind energy applications

Authors	Year	Objective	Strategy	Configuration	Actuator type	Control type	Localization	Reynolds number	Energy authority criteria	Metrics	Key conclusions
Baleriola et al.	2016	Load control	Circulation control	2D translating *NACA 65(4)-421 CC* : modified rounded TE	DBD plasma actuator	Open loop	On rounded TE: different positions examined	2×10^5	C_L and C_L/C_D vs incidence: pressure measurements—actuation flow field analysis without and with inflow	$\Delta C_L = \pm 0.08$	Effectiveness of control was shown through load and pressure measurements
Braud et al.	2016	Load control	Circulation control	2D translating *NACA 65(4)-421 CC* : modified rounded TE	Distributed square microjets (3D effects)	Open loop	96% of chord	2×10^5	ΔC_L vs $C\mu$, flow field survey	$\Delta C_{Lmax} = +0.25$	Microjet distribution on a rounded trailing edge allowed lift manipulation: necessity to investigate the mechanisms of actuation
Brownstein et al.	2014	Stall delay and increase lift	Flow separation	2D translating *GOE 735* airfoil	Dual 2D plasma	Open loop	Suction side ($x/c = 0.5$ and 0.7)	1.5×10^5	ΔC_{Lmax} vs. plasma actuator thrust	$\Delta C_{Lmax} = +0.3$	No influence of the actuator frequency, only the thrust produced by the actuator plays a role (momentum addition)
Chawla et al.	2014	Stall delay and increase lift	Flow separation	2D translating *NACA0012* and *S814* airfoils	Suction slit	Open loop	Suction side ($0.12 < x/c < 0.64$)	8×10^4–4.8×10^5	C_L and C_D vs. $C\mu$	$+0.5 < \Delta C_{Lmax} < +1.3$	Controlled aerodynamic loads are integrated in a BEM computation to model a small HAWT. Ratio wind turbine power/supplied power from 10 to 100
Cooney et al.	2009	Load control and stall delay	Circulation and flow separation	2D translating S827 airfoil	DBD at TE et LE	Open loop	TE/LE suction side	3.83×10^5	ΔC_L for angle of attacks between 1° and 6°: pressure measurements	Average ΔC_L=0.075≈15% increase	ΔC_L obtained by DBD at TE is of the same order as required for gust response at optimal TSR

Table 1 (continued)

Authors	Year	Objective	Strategy	Configuration	Actuator type	Control type	Localization	Reynolds number	Energy authority criteria	Metrics	Key conclusions
Cooney et al.	2016	Stall delay and increase lift	Flow separation	2D translating airfoil + 3D rotating airfoils on *VP-20* (20 kW WT)	2D plasma : double row of electrodes	Open loop	Suction side (from mid-chord to TE)	1×10^5–2×10^5	C_L and ΔC_L vs. DBD voltage for 2D airfoil Power performance increase for 3D rotating airfoil	$+0.06 < \Delta C_L < +0.12$	Field testing. 2–6% of power gain for the VP-20 WT but results are not converged
Cooperman et al.	2014	Decrease lift variation with freestream velocity change	Circulation control	2D modified translating S819: simulated gusts and random wind	microtabs (experiment) and blowing jets (numerical)	Open and closed-loop	Microtabs: 80% chord suction side and 90% chord pressure side: microjets: 95% chord suction and pressure side	1×10^6	ΔC_L: pressure difference at $x/c = 0.25$ (input) and difference between measured and assigned lift (output) in closed loop	$\Delta C_L \approx \pm 0.18$ or 0.19 with microtabs and blowing jets	Closed-loop control systems with microtabs (exp.) and microjets (CFD). Wind tunnel tests (microtabs) and computation (microjets) show a reduction of the deviation from the desired value of lift by 70–80% on airfoil subjected to air speed changes
Feng et al.	2012	Increase lift with small drag penalty	Circulation control	2D translating NACA 0012	DBD on static Gurney flaps with size 3, 4.5 and 7% of chord	Open loop	TE	2×10^4	ΔC_L and ΔC_D for C_μ between 0.04 and 0.014: plain airfoil, with GF and with GF + DBD—velocity field and wake survey	$\Delta C_{L\text{-}GF}$=0.5+extra $\Delta C_{L\text{-}DBD}$=0.18 maximum	Lift (and drag) increased with GF and more with plasma-GF reduce dominant shedding frequency of wake vortex and power spectral peak

Table 1 (continued)

Authors	Year	Objective	Strategy	Configuration	Actuator type	Control type	Localization	Reynolds number	Energy authority criteria	Metrics	Key conclusions
Holst et al.	2015	Load control and performance increase	Circulation control	3D effects on 2D translating FX 63-137 airfoil. 3D simulation with rotation	Finite width Gurney flaps	Open loop	TE	1.35×10^5	Frequencies and velocity in the wake: simulated power vs velocity curve for NREL phase VI and NREL 5 MW subjected to inflow fluctuations	Small WT: increase power: large WT: GF effects compare with lift variation	GF control power without pitch on small WT–large WT: estimation of the effect of an active GF revealed a significant reduction in the probability of extreme changes in lift
Jukes	2015	Stall delay and decrease drag	Flow separation	3D rotating *NREL S822* airfoils	Dual 2D plasma and plasma VGs	Open loop	Suction side (leading edge to $x/c = 0.38$	4×10^4–6.4×10^4	ΔC_P due to drag vs. tip speed ratio and control type	$-24\% < \Delta C_P$ due to drag $<8\%$	Reduction of the torque due to drag up to 24%. Plasma VGs can be efficient when used in off-design conditions radial body force generated by plasma VGs are important in rotating separated flows
Kotsonis et al.	2014	Dynamic lift manipulation	Circulation control	2D translating NACA 64-2-A015 with rounded circular trailing edge	DBD plasma actuator	Open loop	On rounded TE: different positions examined	1.4×10^5–2.8×10^5	ΔC_L and ΔC_D: flowfield topology—POD analysis	ΔC_L max 0,1 at 10 m/s	Analysis of the effect of the actuator and its position on the airfoil lift on the topology and characteristics of the wake flow field

Table 1 (continued)

Authors	Year	Objective	Strategy	Configuration	Actuator type	Control type	Localization	Reynolds number	Energy authority criteria	Metrics	Key conclusions
Maldonado et al.	2010	Stall delay to reduce blade vibrations	Flow separation	3D translating *NACA4415* airfoil. Finite wind turbine blade	Synthetic jet arrays	Open and closed-loop	Suction side ($x/c = 0.25$)	7.1×10^4–2.4×10^5	Aero loads and vibrations vs. C_μ and frequency	$\Delta C_{\mathrm{Lmax}} = +0.12$	Reduce separation and vibration. A tip action can be as efficient as a more distributed action regarding the vibration reduction
Nelson et al.	2008	Stall delay and increase lift, reduce load fluctuations	Circulation and flow separation	2D translating S827 and S822 airfoils	2D plasma and plasma VGs	Open loop	Suction side 2D actuators at LE ($x/c = 0.78$) 3D actuators at TE ($0 < x/c < 0.2$)	4×10^5	ΔC_{L} vs. angle of attack and actuator types	$\Delta C_{\mathrm{L}} = +0.08$	Increase the lift as the flow is attached with 2D actuators located close to the trailing edge and additionally delay the stall with 3D actuators located close the leading edge. Suggest that the actuator effects are additive
Niether et al.	2015	Reduce load fluctuations	Flow separation	2D translating DU97-W-300 airfoil	Adaptive steady blowing jet array	Open loop	Suction side ($0.22 < x/c < 0.46$)	2.2×10^5	C_{L} vs. angle of attack and injected mass flow, load fluctuation alleviation	$\Delta C_{\mathrm{Lmax}} = +0.2$	Blowing jet location is naturally adapted by the pressure distribution on the suction side. Can smooth out the lift curve close to the stall. Demonstration of load fluctuation alleviation is given through numerical simulation of the NREL 5 MW reference rotor

Table 1 (continued)

Authors	Year	Objective	Strategy	Configuration	Actuator type	Control type	Localization	Reynolds number	Energy authority criteria	Metrics	Key conclusions
Nikoueeyan et al.	2014b	Dynamic stall and load control	Circulation and dynamic stall control	2D DU97-W-300 modified with thick TE - translation and periodic pitch motions	GF 5% of chord up and down on thick TE	Open loop	Gurney flap on 10% of chord	4.3×10^5	Pressure on both sides: C_L and C_M by integration—velocity field	$\Delta C_L \approx \pm 0.5$ to 0.7	Significant control authority in static conditions and in moderate dynamic stall conditions. In deep stall conditions, some effectiveness for C_L and C_m hysteresis reduction
Pechlivanoglou et al.	2010	Load control and Power regulation	Lift control	2D translating DU96 W 180 airfoil with a flexible flap	20% of chord high deflection flexible flap	Open loop	TE	1.3×10^6	C_L, C_D and C_m vs incidence for positive and negative flap deflections	$\Delta C_L \approx \pm 0.8$	Feasibility of implementation of high deflection flexible flap structures for aerodynamic control and power regulation of wind turbine rotors
Pechlivanoglou	2013	Stall delay and increase lift, reduce load fluctuations	Circulation and flow separation	2D translating airfoils (4 types)	Set of 14 actuators	Open loop	TE and LE, spanwise distribution	1.3×10^6	Lift and load fluctuation vs. Angle of attack and actuator type	Load fluctuation reduction 52% with flexible flaps	Estimation of the overall performance of 14 actuators according to different technical fields. Design concept of a *smart blade* with optimized distribution of actuators
Shun and Ahmed	2012	Stall delay to reduce blade vibrations	Flow separation	2D translating NACA 63-421 airfoil	Air jet vortex generators	Open loop	Suction side ($x/c = 0.125$)	6.4×10^5	ΔC_L vs. Cμ	$+0.023 < \Delta C_L < +0.18$	Better efficiency with exponential nozzle

Table 1 (continued)

Authors	Year	Objective	Strategy	Configuration	Actuator type	Control type	Localization	Reynolds number	Energy authority criteria	Metrics	Key conclusions
Stalnov et al.	2010	Stall delay	Flow separation	2D translating modified IAI Pr8-SE airfoil	Synthetic jet actuator slots	Open loop	Suction side ($x/c = 0.375$)	2×10^5–8×10^5	ΔC_L vs. α, reduced frequency and C_μ. Wind energy-oriented figure of merit	$\Delta C_L = +0.25$; AFM3 = 1.8	Wind energy-oriented figure of merit, giving an assessment of the overall energy efficiency gains (5–15%)
Tanaka et al.	2013	Stall delay and increase lift	Flow separation	3D rotating airfoils on a 30 kW WT (NACA and DU airfoils)	2D plasma	Open loop	Leading edge	10^5	Power production vs. tip speed ratio and plasma actuation	$\Delta C_{Power} = +0.2$	Control efficiency at full scale even in highly turbulent conditions. Needs to be statistically proved
Troshin and Seifert	2013	Recover degraded performance and reduce load fluctuations	Flow separation	2D translating modified AH93-W-300 airfoil	Synthetic jet arrays	Open and closed loop	Suction side ($0.2 \leq x/c \leq 0.8$)	4×10^5–5×10^5	ΔC_L and ΔC_D vs. α, reduced frequency and C_μ. Wind energy-oriented figure of merit	$\Delta C_L = +0.27$; $\Delta C_D = -0.06$ AFM3 = 1.6	Energy harvesting capability of a degraded airfoil is expected to be increased by up to 60%
Vries de	2014	Load control	Circulation	2D translating NACA 0018	Synthetic jet blowing perpendicularly to wall	Open loop	Two positions: 88 and 98.5% of chord	Max 5.5×10^5	Computed time-averaged ΔC_L and ΔC_D for reduced frequency $F+$ between 1 and 30 and C_μ between 0.65 and 1.31	$\Delta C_L \approx 0.3$: time response ≈12 chords	No experimental results due to degradation of synthetic jets performance at high actuation frequencies of interest. Computational results showed synthetic jet could be used for load control, with performance reduction at high angles of attack

Table 1 (continued)

Authors	Year	Objective	Strategy	Configuration	Actuator type	Control type	Localization	Reynolds number	Energy authority criteria	Metrics	Key conclusions
Wang et al.	2011	Stall delay and reduce load fluctuations	Flow separation	2D translating custom airfoil	Unsteady blowing slots	Open and closed loop	Suction side ($x/c = 10, 50$ and 85%)	1.2×10^5	C_L vs. angle of attack and actuation. Reduction of standard deviation of lift fluctuations	$\Delta C_{Lmax} = +0.05$, Lift_rms decrease 12%	Needs to close the control loop with a pressure sensor at the LE to reduce lift fluctuations more efficiently

References

Baleriola S, Leroy A, Loyer S, Devinant P, Aubrun S (2016) Circulation control on a rounded trailing-edge wind turbine airfoil using plasma actuators. J Phys Conf Ser 753(5):52001

Barlas TK, van Kuik GAM (2010) Review of state of the art in smart rotor control research for wind turbines. Prog Aerosp Sci 46(1):1–27

Ben-Harav A, Greenblatt D (2016) Plasma-based feed-forward dynamic stall control on a vertical axis wind turbine. Wind Energy 19(1):3–16

Berg DE, Zayas JR, Lobitz DW, van Dam CP, Chow R, Baker JP (2007) Active aerodynamic load control of wind turbine blades. In: ASME/JSME 2007 5th joint fluids engineering conference, Volume 2: Fora, Parts A and B. San Diego, California, USA, July 30–August 2, 2007. ISBN 0-7918-4289-4

Berg JC, Barone MF, Yoder NC (2014) SMART wind turbine rotor: data analysis and conclusions. SANDIA REPORT SAND2014-0712. https://www.energy.gov/sites/prod/files/smart_wind_turbine_data.pdf

Braud C, Guilmineau E (2016) Jet flow control at the blade scale to manipulate lift. J Phys Conf Ser 753(2):022031

Brownstein ID, Szlatenyi CS, Breuer KS (2014) Enhanced aerodynamic performance of a wind turbine airfoil section using plasma actuation. AIAA Paper 2014-1244

Burton T, Sharpe D, Jenkins N, Bossanyi E (2001) Wind energy handbook. Wiley, Chichester

Cattafesta LN III, Sheplak M (2011) Actuators for active flow control. Annu Rev Fluid Mech 43:247–272

Chawla JS, Suryanarayanan S, Puranik B et al (2014) Efficiency improvement study for small wind turbines through flow control. Sustain Energy Technol Assess 7:195–208. doi:10.1016/j.seta.2014.06.004

Chen H, Qin N (2017) Trailing-edge flow control for wind turbine performance and load control. Wind Energy 105:419–435

Cooney J (2009) Feasibility of plasma actuators for active flow control over wind turbine blades. AIAA Paper 2009-218

Cooney J, Szlatenyi CS, Fine NE (2016) The development and demonstration of a plasma flow control system on a 20 kW wind turbine. AIAA Paper 2016-1302

Cooperman AM, van Dam CP (2015) Closed-loop control of a microtab-based load control system. J Aircr 52(2):387–394

Cooperman A, Blaylock M, van Dam CP (2014) Experimental and simulated control of lift using trailing edge devices. J Phys Conf Ser 555(1):012019

Counihan J (1975) Adiabatic atmospheric boundary layers: a review and analysis of data from the period 1880–1972. Atmos Environ 9:871–905

Crowther WJ, Jabbal M, Liddle SC (2010) Flow control fallacies: a review of common pitfalls in flow control research. Proc IMechE Part G J Aerosp Eng 225(1):1–11

De Vries H, van der Weide ETA, Hoeijmakers HWM (2014) Synthetic jet actuation for load control. J Phys Conf Ser 555(1):12026

Ekaterinaris JA (2004) Prediction of active flow control performance on airfoils and wings. Aerosp Sci Technol 8:401–410. doi:10.1016/j.ast.2004.02.003

ESDU Engineering Sciences Data Unit (1985) Characteristics of atmospheric turbulence near the ground. Item No 85020, ISBN 978 0 85679 526 8

ETIP Wind (2016) Strategic research and innovation agenda. 2016. https://etipwind.eu/files/reports/ETIPWind-SRIA-2016.pdf

Feng LH, Jukes TN, Choi KS, Wang JJ (2012) Flow control over a NACA 0012 airfoil using dielectric-barrier-discharge plasma actuator with a Gurney flap. Exp Fluids 52(6):1533–1546

Ferreira et al (2016) Results of the AVATAR project for the validation of 2D aerodynamic models with experimental data of the DU95W180 airfoil with unsteady flap. J Phys Conf Ser 753:022006

Greenblatt D, Lautman R (2015) Inboard/outboard plasma actuation on a vertical-axis wind turbine. Renew Energy 83:1147–1156. doi:10.1016/j.renene.2015.05.020

Greenblatt D, Schulman M, Ben-Harav A (2012) Vertical axis wind turbine performance enhancement using plasma actuators. Renew Energy 37:345–354. doi:10.1016/j.renene.2011.06.040

Gross A, Fasel HF (2012) Flow control for NREL S822 wind turbine airfoil. AIAA J 50:2779–2790. doi:10.2514/1.J051628

Holst D, Bach AB, Nayeri CN, Paschereit CO, Pechlivanoglou G (2015) Wake analysis of a finite width gurney flap. J Eng Gas Turbines Power 138(6):62602

Johnson SJ, van Dam CP, Berg D (2008) Active load control techniques for wind turbines. SANDIA REPORT SAND2008-4809. http://windpower.sandia.gov/other/084809.pdf

Johnson SJ, Baker JP, van Dam CP, Berg D (2010) An overview of active load control techniques for wind turbines with an emphasis on microtabs. Wind Energy 13:239–253

Jonkman J, Butterfield S, Musial W, Scott G (2009) Definition of a 5-MW reference wind turbine for offshore system development. Tech rep NREL, NREL/TP-500-38060

Jukes TN (2015) Smart control of a horizontal axis wind turbine using dielectric barrier discharge plasma actuators. Renew Energy 80:644–654. doi:10.1016/j.renene.2015.02.047

Kaimal JC, Finnigan JJ (1994) Atmospheric boundary layer flows, their structure and measurements. Oxford University Press, Oxford

Kotsonis M, Pul R, Veldhuis L (2014) Influence of circulation on a rounded-trailing-edge airfoil using plasma actuators. Exp Fluids 55(7):1772

Maldonado V, Farnsworth J, Gressick W, Amitay M (2010) Active control of flow separation and structural vibrations of wind turbine blades. Wind Energy 13:221–237. doi:10.1002/we.336

Meijerink JAW, Hoeijmakers HWM (2011) Plasma actuators for active flow control on wind turbine blades. AIAA Paper 2011-3353

Mücke T, Kleinhans D, Peinke J (2010) Atmospheric turbulence and its influence on the alternating loads on wind turbines. Wind Energy 14(2):301–316

Nelson RC, Corke TC, Othman H, et al. (2008) A smart wind turbine blade using distributed plasma actuators for improved performance. AIAA Paper 2008-1312

Niether S, Bobusch B, Marten D et al (2015) Development of a fluidic actuator for adaptive flow control on a thick wind turbine airfoil. J Turbomach 137:61003. doi:10.1115/1.4028654

Nikoueeyan P, Strike JA, Magstadt AS, Hind MD, Naughton JW (2014a) Gurney flap control authority on a pitching wind turbine airfoil. AHS 70th annual forum proceedings, May 2014, pp 3147–3161. SKU #: 70-2014-0103

Nikoueeyan P, Strike JA, Magstadt AS, Hind MD, Naughton JW (2014b) Aerodynamic response of a wind turbine airfoil to Gurney flap deployment. AIAA Paper 2014-2146

Pechlivanoglou G (2013) Passive and active flow control solutions for wind turbine blades. PhD Dissertation, Technical University of Berlin

Pechlivanoglou GK, Wagner J, Nayeri CN, Paschereit CO (2010) Active aerodynamic control of wind turbine blades with high deflection flexible flaps. AIAA Paper 2010-644

Peinke J, Barth S, Böttcher F, Heinemann D, Lange B (2004) Turbulence, a challenging problem for wind energy. Phys A 338:187–193

Pereira R, van Bussel GJW, Timmer WA (2014) Active stall control for large offshore horizontal axis wind turbines; a conceptual study considering different actuation methods. J Phys Conf Ser 555:12082. doi:10.1088/1742-6596/555/1/012082

Sathe A, Mann J, Barlas T, Bierbooms W, van Bussel GJW (2013) Influence of atmospheric stability on wind turbine loads. Wind Energy 16:1013–1032

Schlipf DJ, Kühn M (2013) Nonlinear model predictive control of wind turbines using LIDAR. Wind Energy 16:1107–1129

Schubel PJ, Crossley RJ (2012) Wind turbine blade design. Energies 5(9):3425–3449

Shun S, Ahmed NA (2012) Wind turbine performance improvements using active flow control techniques. Procedia Eng 49:83–91. doi:10.1016/j.proeng.2012.10.115

Somers DM (1997) Design and experimental results for the S809 airfoil. Tech rep NREL, NREL/SR-440-6918

Stalnov O, Kribus A, Seifert A (2010) Evaluation of active flow control applied to wind turbine blade section. J Renew Sustain Energy 2:063101

Tanaka M, Amemori K, Matsuda H, et al. (2013) Field test of plasma aerodynamic controlled wind turbine. In: EWEA conference, February 4–7, 2013, Vienna, Austria

Troshin V, Seifert A (2013) Performance recovery of a thick turbulent airfoil using a distributed closed-loop flow control system. Exp Fluids 54:1443

Van Kuik J et al (2016) Long-term research challenges in wind energy—a research agenda by the European Academy of Wind Energy. Wind Energ Sci 1:1–39

Vey S, Marten D, Pechlivanoglou G, Nayeri CN, Paschereit CO (2015) Experimental and numerical investigations of a small research wind turbine. AIAA Paper 2015-3392

Wagner R, Pedersen TF, Courtney M, Antoniou I, Davoust S, Rivera RL (2014) Power curve measurement with a nacelle mounted lidar. Wind Energy 17:1441–1453

Walker S, Segawa T (2012) Mitigation of flow separation using DBD plasma actuators on airfoils: a tool for more efficient wind turbine operation. Renew Energy 42:105–110. doi:10.1016/j.renene.2011.09.001

Wang G, Walczak J, Elhadidi B, Glauser M (2011) Preliminary investigation of the active flow control benefits on wind turbine blades. AIAA Paper 2011-3611

Wetzel DA, Griffin J, Cattafesta LN (2013) Experiments on an elliptic circulation control aerofoil. J Fluid Mech 730:99–144

Xu HY, Qiao CL, Ye ZY (2016) Dynamic stall control on the wind turbine airfoil via a co-flow jet. Energies 9(6):429

Zhang M, Yu W, Xu J (2014) Aerodynamic physics of smart load control for wind turbine due to extreme wind shear. Renew Energy 70:204–210